Commissioning of RPC detector systems for the Daya Bay Experiment

Zhe Ning[a,b], Qingmin Zhang[c,1], Jiawen Zhang[a], Jilei Xu[a], Logan Lebanowski[d], Miao He[a], Jiaheng Zou[a], Changgen Yang[a], Jie Zhao[a,b], Huifeng Hao[e], Lei Zheng[e], Xiaolu Ji[a], Fei Li[a], Jun Xu[a], Viktor Pěč[g], Mengyun Guan[a], Yuen-Keung Hor[h], Kwong Lau[d], Shih-Kai Lin[d], Jonathan Link[h], Changguo Lu[f], Yue Meng[h], Sen Qian[a], Bedrich Roskovec[g], Vit Vorobel[g]

[a]Institute of High Energy Physics, Chinese Academy of Sciences, Beijing 100049, China
[b]Graduate University of the Chinese Academy of Sciences, Beijing 100049, China
[c]Xi'an Jiaotong University, Xi'an 710049, China
[d]Department of Physics, University of Houston, Houston, TX 77204-5005, USA
[e]University of Science and Technology of China, Hefei 230026, China
[f]Department of Physics, Princeton University, Princeton, NJ 08544, USA
[g]Faculty of Mathematics and Physics, Charles University, Prague 12116, Czech Republic
[h]Center for Neutrino Physics, Virginia Tech, Blacksburg, VA 24061, USA

Abstract：

The commissioning of the three Resistive Plate Chamber (RPC) muon detector systems of the Daya Bay Neutrino Reactor Experiment began in April, October and November, 2011, in Experimental Hall 1, 2 and 3 (EH1, EH2 and EH3), respectively. During commissioning, all sub-systems, including RPC modules, electronics, High Voltage (HV), gas, online Data Acquisition (DAQ) and offline software, were tested and tuned. Optimal operational conditions were determined and finally, all three RPC systems began taking combined data with all other sub-detectors at the three experimental sites on December 24, 2011. RPC performance, such as efficiency and noise rate, determined from the earliest combined data runs is reported here.

PACS: 29.40.-n; 29.40.Cs

Key words：RPCs; muon veto detectors; commissioning; Daya Bay

1. Introduction

The Daya Bay Reactor Neutrino Experiment [1] aims at the precise measurement of the neutrino mixing angle θ_{13} by comparing observed Inverse Beta Decay (IBD) event rates at various baselines from six nuclear reactors. At Daya Bay, there are three Experiment Halls (EHs): two near halls (EH1 and EH2) and one far hall (EH3).The most recent result from the Daya Bay Experiment is $\sin^2 2\theta_{13} = 0.089 \pm 0.010(\text{stat.}) \pm 0.005(\text{syst.})$ [2]. The majority of the uncertainty in θ_{13} is due to

[1]Corresponding Author, zhangqingmin@mail.xjtu.edu.cn

backgrounds induced by cosmic-ray muons. To minimize these uncertainties, the Antineutrino Detectors (ADs) are deployed underground with redundant muon veto systems. A muon veto system consists of a water Cherenkov pool and an RPC detector array. As shown in Fig. 1, the ADs [3] are immersed in the water pool, which identifies muons and shields from ambient radioactivity. The RPCs are located above the water pool and independently detect muons.

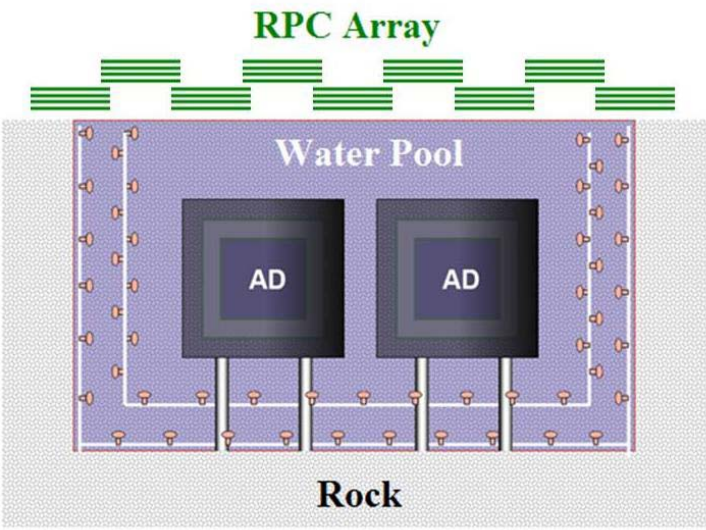

Fig. 1 Layout of sub-detectors at one site

The RPC has been applied widely in high energy physics experiments such as BaBar [4], Belle [5], ALICE [6], ATLAS [7], CMS [8] since its invention in 1980s [9]. Bakelite RPCs, developed by Institute of High Energy Physics, Chinese Academy of Sciences (IHEP), have been successfully applied in BESIII as a muon identifier [10, 11, 12]. Based on experience from BESIII and pre-studies implemented to meet the specific requirements of Daya Bay Reactor Neutrino Experiment, RPC technology was adopted to construct an underground cosmic-ray detector made of RPCs [13].

2. Components of the RPC detector system

An RPC detector system is composed of RPC modules, a gas system, a HV system and an electronic readout system. In addition, a Detector Control System (DCS) is used to monitor and control the gas and HV systems as well as monitor environmental temperature, pressure and humidity.

2.1 The RPC modules

The RPC arrays in both EH1 and EH2 consist of 6 × 9 modules (9 × 9 modules in EH3). The RPC modules are deployed on a movable support structure as can be seen in Fig. 2. During commissioning, the RPC array stayed in an 'RPC hall' to the side of the pool, while it was moved to the designed position along the RPC support railway during normal data-taking. At each site, two telescope RPC modules are installed at two opposing banks of the water pool, approximately 2.0 m above the top of the RPC array (see Fig. 2).

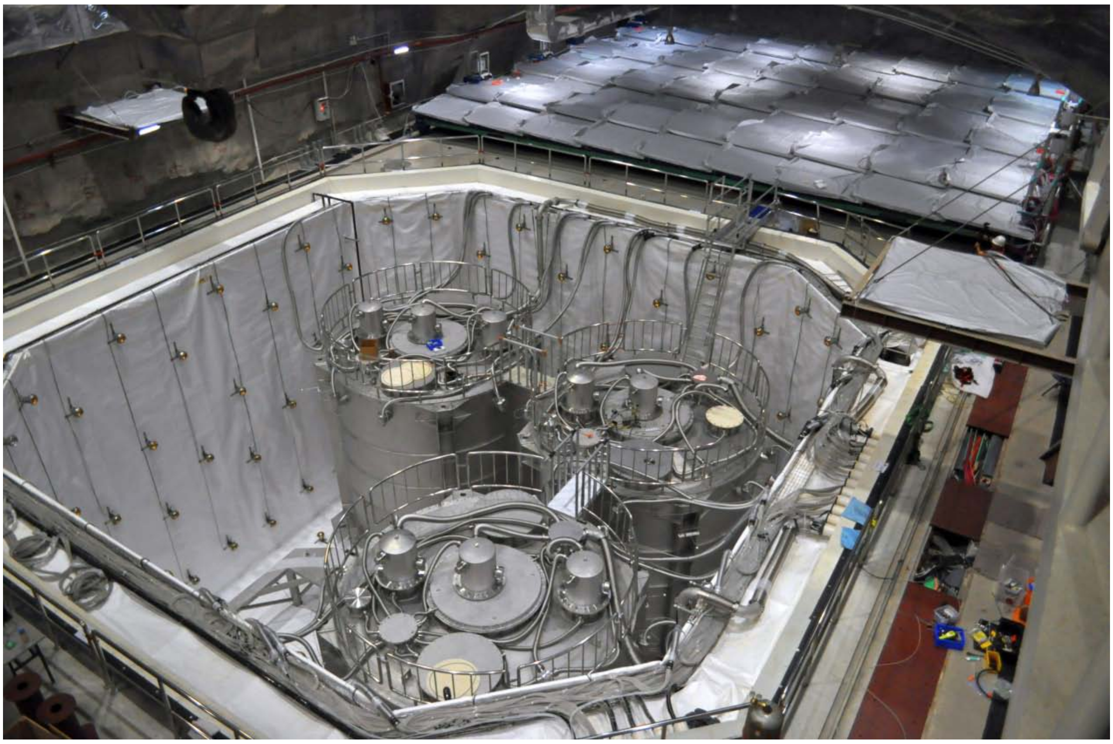

Fig. 2 EH3: RPC array in the RPC hall. It moves to/away from the top of the water pool by motor and railway.

Fig. 3 shows the relative position of adjacent RPC modules. The 10 cm overlap on all sides among adjacent modules aims to minimize dead regions. Module dimensions are 2.17 × 2.20 × 0.08 m^3. The inner structure of modules is shown in Fig. 4. Each module consists of 4 layers and each layer contains one 'small' bare RPC (1.00 × 2.10 m^2) and one 'big' bare RPC (1.10 × 2.10 m^2), as shown in the top right of Fig. 4. Furthermore, the placement of the two chambers varies among layers to reduce overlapping dead regions (0.024 × 2.10 m^2).

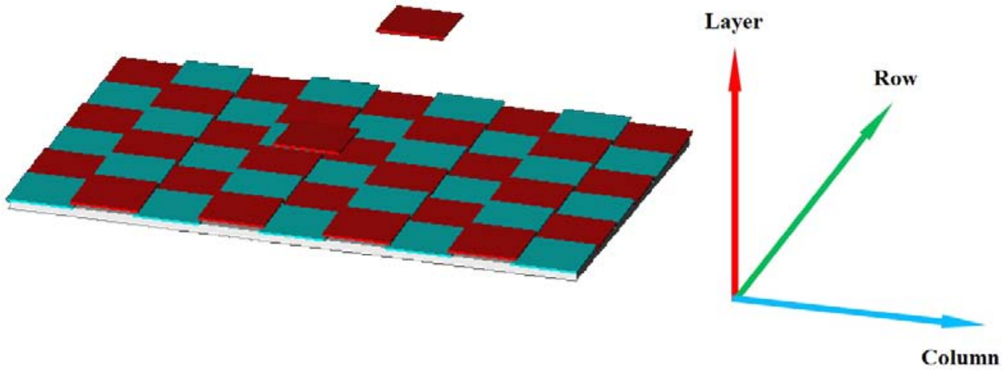

Fig. 3 Layout of RPC modules

RPC signals are readout from copper-clad sheets of FR-4. Each sheet is cut into four readout strips, each 2.1 m × 0.26 m, with a zigzag design as shown in the bottom right of Fig. 4. The performance of this type of readout strip is equivalent to one with dimensions 8.4 m × 6.25 cm. This zigzag design changes the impedance to give a taller and narrower pulse, which would otherwise require more readout channels [14]. One end of each strip is connected to the input of a Front-End Circuit (FEC) while both ends are connected to a clean ground through a 27 Ω resistor. Two sheets of readout strips cover each layer of RPCs, giving each module a total of 32 readout strips (4 strips/sheet × 2 sheets/layer × 4 layers). As illustrated in Fig. 4, strips on the 1st and 4th layers (counting from the bottom) are in the 'X' direction, and the strips on the 2nd and 3rd layers are in the 'Y' direction, which is parallel to the RPC support railway.

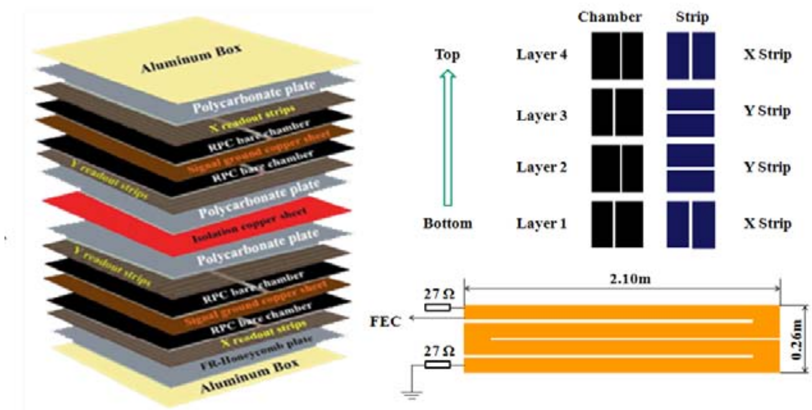

Fig. 4 The inner structure of an RPC module

2.2 Gas system

As shown in Fig. 5, the gas system consists of gas cylinders, a gas mixing and fire/detector safety monitoring system, a gas distribution system and a gas chromatograph at each site. Daya Bay RPCs operate in streamer mode with the gas mixture argon argon: R134a: iso-butane: SF_6 = 65.5: 30: 4: 0.5 [15] and is controlled by an MKS 247D system. The flow rate at each site is about one volume per day per four RPCs, corresponding to total system flow rates of 1622, 1716 and 2172 sccm in EH1, EH2 and EH3, respectively. The status of the gas system is monitored remotely using the DCS. If any gas flow rate is not within the expected range, the gas system will shut down automatically and send an alarm signal to the DCS. The gas mixture is analyzed every two hours by a local gas chromatograph (Varian GC430) at each site, ensuring the correct gas mixture.

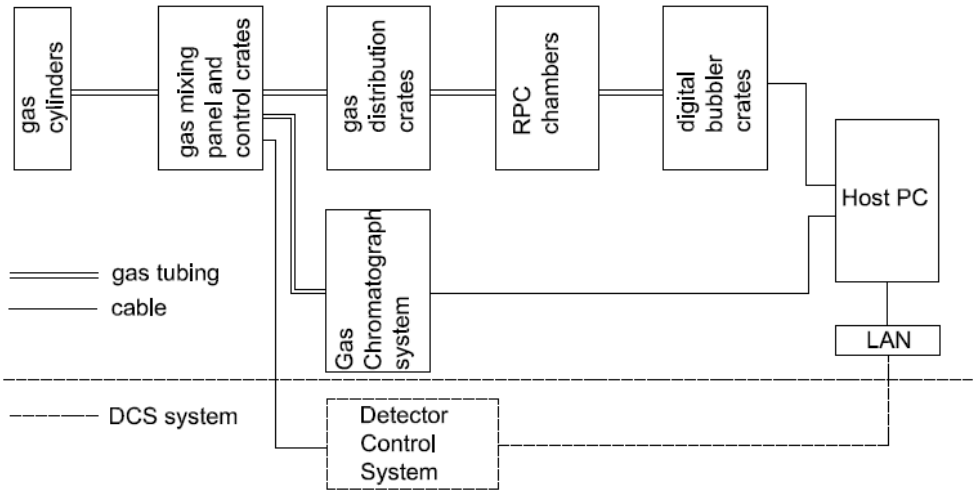

Fig. 5 The architecture of RPC gas system

2.3 High Voltage system

Each High Voltage (HV) system uses four CAEN [16] HV cards (two －4kV A1733N and two ＋6kV A1732P), each with twelve channels, in EH1 and EH2 (there are six cards in EH3). Each HV channel is divided into 9 channels by a fan-out box and then distributed to RPCs through an HV interface box attached to the outside of each RPC module. Accordingly, each HV main frame channel supplies power to a total of 18 RPCs of the same layer in 9 consecutive RPC modules (there are two RPCs per layer). The entire HV system is also monitored and controlled remotely by DCS. Moreover, the two DCS controls of the HV and Gas systems are interlocked for the safety of the RPCs. In the case of an alarm signal from the gas system, DCS will warn control room personnel and allow them 30 minutes to address the alarm before automatically turning off the RPC HV.

2.4 Readout Electronics system

In each hall, the electronics system consists of FECs, ReadOut Transceivers (ROTs), a VME crate and two VME modules, including an RPC Trigger Module (RTM) and a ReadOut Module (ROM) [17]. A detailed diagram is shown in Fig. 6. The 32 signal strips in each RPC module are read out by a single FEC. The hit information (1 or 0) for every channel is obtained by discriminating the signal with the internal discriminators of the FECs. If three or all four layers within one RPC module have hits simultaneously, a local trigger will be generated by the FEC (a ‘3/4’ trigger), and then sent to the RTM through an ROT, which transmits the FEC data to the ROM or the RTM. At the same time the FEC data is temporarily stored in a shift register. Upon the arrival of the readout trigger from the RTM, the FEC data is transferred to an event buffer. In order to match the RTM readout trigger (25 ns/clock cycle × 16 clock cycles) with its corresponding FEC data, an adjustable latency time is introduced. A proper latency setting has been determined onsite through testing (see Section 4.2) and is configurable through the DAQ system. The resulting data are buffered in the ROM before being transmitted to the DAQ system by VME bus. In addition to locally generated 3/4 triggers, which only read out a single RPC module, a periodic forced trigger reads out all hit information from all FECs at 10 Hz during normal data taking in order to measure RPC noise rate. The DAQ system reads out the data packages by the means of polling and sorts them online according to time stamps [18].

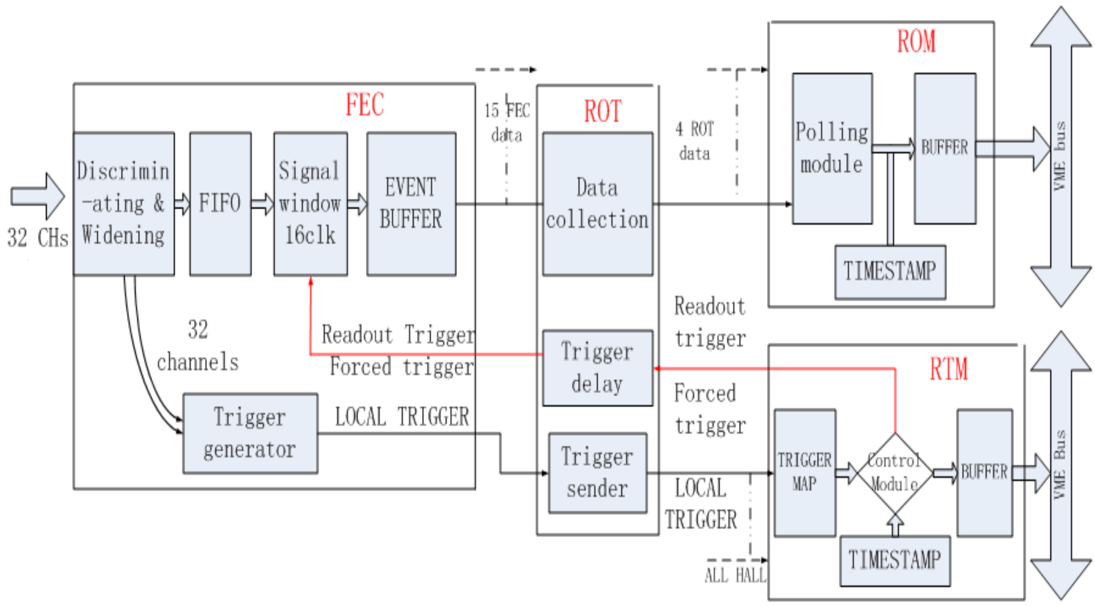

Fig. 6 The architecture of RPC electronics system

3. Software of the RPC system

RPC software includes online and offline software. The former is used to monitor performance during data-taking, and the latter is used for detector calibration and physics analysis.

3.1 Software introduction

FEC data is acquired and sorted by the online DAQ system, and then analyzed by the offline software. The trigger rates in EH1, EH2, and EH3 are respectively ~ 210Hz, ~140Hz, and ~50Hz with a 10Hz forced trigger included. By checking the online hit map in the DAQ system, dead or hot channels could be found in real time. More detailed information, including efficiency and noise rate, is provided by performance quality monitoring software that runs while data is being taken.

RPC offline software [19] includes simulation [20], detector calibration and event reconstruction, and runs in the Daya Bay NuWa framework, which was developed based on Gaudi [21]. Muon simulation data is generated using Geant4 and surveyed mountain geometry. Experimental data are converted to physics events, which include event time, trigger type (3/4 or 2/4 trigger type, the latter being from the original design and unused) and a list of hits with coordinates. Physics events are analyzed based on the Lightweight Analysis Framework [22] offline software framework and used to calibrate detector performance and reconstruct muon information (incident positions or/and tracks). Simulation results and analytical methods are validated and tuned by comparison with experimental data.

3.2 Detector calibration

The offline calibration of RPC performance includes determination of the efficiency and noise rate of each layer in an RPC module. The calibration algorithms have been developed to account for the structure of an RPC module, layout of RPC modules, readout mechanism and the anchoring position of an RPC array, and will be described in the following sections.

3.2.1 Efficiency

Since the RPC detector is used as a muon veto detector in the Daya Bay Experiment, precise determination of muon efficiency is the key. The RPC layer efficiency is calculated as follows:

$$\varepsilon_i = \frac{N_{4-fold,ijkl,WP}}{N_{3-fold,jkl,WP}}, \quad (1)$$

where ε_i is the efficiency of layer *i* in a given module, $N_{4-fold,ijkl,WP}$ is the number of 4-layer coincidences and $N_{3-fold,jkl,WP}$ is the number of 3-layer coincidences involving layers *j*, *k* and *l*. The meaning of *WP* is explained below.

Given that a trigger must have three or more layers with hits, RPC module efficiency is calculated as follows:

$$\varepsilon_{3/4} = \prod_{i=1}^{4} \varepsilon_i + \sum_{i=1}^{4} (1-\varepsilon_i) \prod_{\substack{j=1 \\ j \neq i}}^{4} \varepsilon_j , \quad (2)$$

where $\varepsilon_{3/4}$ is the module efficiency in 3/4 trigger mode.

In order to cleanly select muons, two requirements are introduced. The first requirement (R1) is that no more than two strips (the two strips should be adjacent if two strips are fired in the same event) are fired in each layer of the triggered modules for every event. The second requirement (R2) is that muon events be tagged by the Water Cherenkov Pools if applicable. R2 reduces the effect of underestimating the efficiency due to accidentals and other backgrounds, which are larger relative to the muon flux underground (0.90 ± 0.06, 0.69 ± 0.08 and 0.046 ± 0.004 Hz/m^2 in EH1, EH2 and EH3, respectively) [19] than to the flux at sea level. During commissioning, the RPC arrays stayed in the RPC halls, not above the water pools, so R2 could not be applied. After commissioning, the RPC arrays were moved over the tops of the water pools. As shown in Fig. 7, when R2 is applied, the calculated efficiency is higher and is consistent with the test results at sea level in IHEP, Beijing [23]. The difference in EH3 is especially obvious due to the lower muon flux. The muon flux is at the same level as the background (0.055, 0.034 and 0.048 Hz/m^2 in EH1, EH2 and EH3, respectively), which includes 3-layers accidentals (from estimates using measured singles rates: 0.0043, 0.0059 and 0.0071 Hz/m^2 in EH1, EH2 and EH3, respectively). According to Monte Carlo simulation, the efficiency bias due to R2, which introduces a muon angle selection bias, is 0.05% (0.07% for EH3).

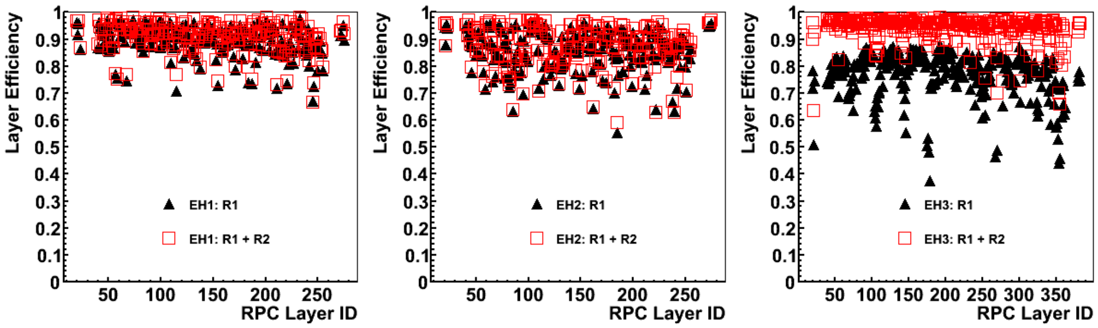

Fig. 7 The effect with water pool muon cut

3.2.2 Noise rate

The RPC noise level is indicated by the noise rate and dark current. The layer noise rate, which can be used for detector monitoring and the estimation of accidentals and purity (the ratio of true muon events in RPC triggers), is defined as below:

$$N_i = \frac{Hit_i}{S \times n \times T}, \tag{3}$$

where N_i is the noise rate of Layer i in one module, Hit_i is the number of noise hits in the investigated layer (during forced triggers), S is the effective area of a layer (2.08 × 2.06 = 4.28 m^2), n is the number of forced triggers, and T is the sampling time of each forced trigger (= width of readout trigger + typical width of signal = 25ns/clock × 16clocks + 150ns = 550ns).

4. RPC Commissioning

During commissioning problems were solved, operational conditions were tuned and analysis software was prepared, so that the RPC systems could meet the design goals. The special techniques used in the Daya Bay experiment are described in the following sections.

4.1 Solutions for a severe operational environment

The Daya Bay Reactor Neutrino Experiment is located in the south of China, 55 km northeast of Hong Kong and 45 km east of Shen Zhen city. The local relative humidity is high throughout the year, especially during summer, when it often surpasses 90%. Since each experimental hall is large, it is difficult to achieve a humidity of 60% or lower. In such conditions, the current of the RPCs is higher than in the tests in Beijing. The solution implemented to address this issue is the flow of dry air directly into each RPC module (surrounding the RPC chambers), controlling the internal operational environment instead of the entire hall. This solution has been very effective at reducing the current and minimizing related HV channel tripping.

As shown in Fig. 8 (a), the dry air system consists of a dry air supplier (compressor) and distributor. Before distribution, the dry air has a relative humidity of 10% and temperature of about 21℃. Fig. 8 (b) shows the current of EH1 RPCs before and after flowing dry air into the RPC modules for 10 days continually. The current was reduced by about 50%.

In addtion, during commissioning, water dropped from the ceilings of the experimental halls and entered some RPC modules, causing their HV channels to trips. Accordingly, every module has been covered with a waterproof and fire-reluntanct cover.

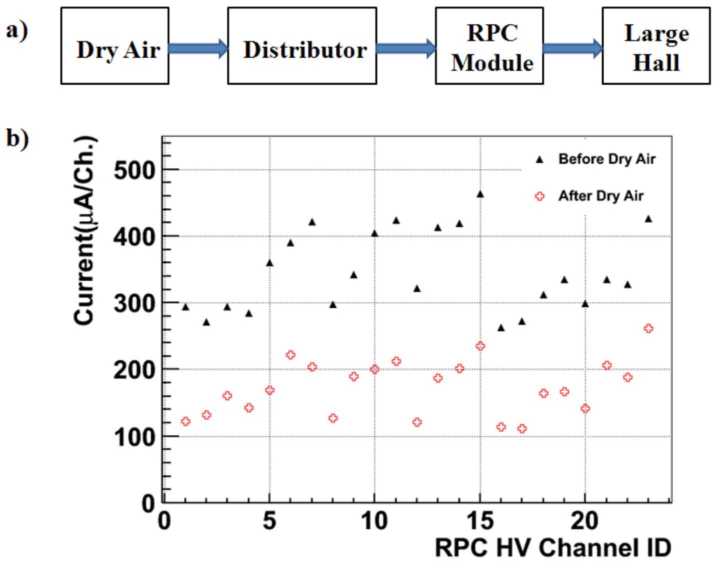

Fig. 8 Dry air setup a) and its effect on RPC current b)

4.2 Latency scan

As described in Section 2.4, a proper latency setting ensures the time matching of the readout trigger and its corresponding FEC data, thus avoiding data loss. This setting can be determined simply by looking at the trigger rate as a function of latency setting (tested under a signal window = 16 clcok cycles). In Fig. 9 it is clearly seen that data loss occurs when the latency is out of the range (45, 60) clock cycles. Accordingly, a latency value of 54 clock cycles was chosen, which is almost in the middle of the usable range.

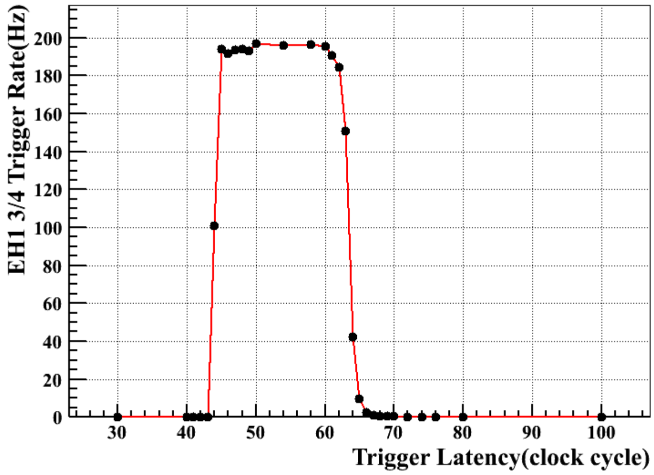

Fig. 9 The trigger rate versus trigger-readout time latency

4.3 Threshold scan

The choice of signal threshold is the result of a balance between maximizing efficiency and maximizing purity (rejecting noise). Using threshold scan data from all three halls (see Fig. 10), we have chosen an optimal threshold of -35 mV. It is seen in Fig. 10 that the efficiency decreases quickly above a threshold of |-40| mV. The slight non-monotonic behavior at around -80 to -100 mV is attributed to environmental fluctuations, to which efficiency is more sensitive at efficiencies closer to 50%. The similar behavior between -20 and -30 mV is simply due to the influence of noise in the determination of efficiency. Thus, for maximal efficiency with minimal noise, the threshold is set at -35 mV in all three halls. Threshold scans done during module testing in Beijing gave -30 mV; however, as described in Section 4.1, the operational environment of Daya Bay is different from that of Beijing.

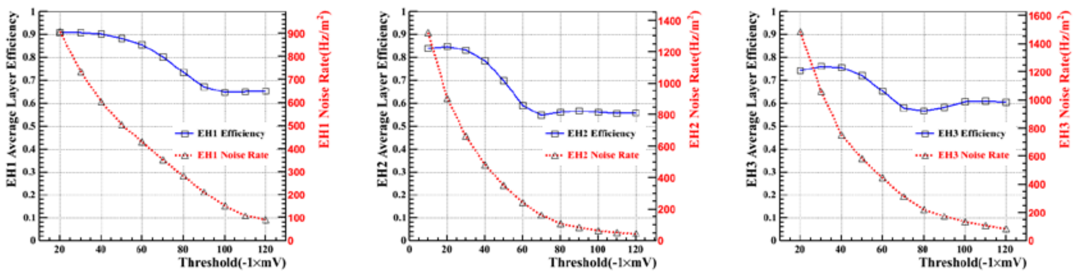

Fig. 10 The average efficiency of all layers of RPCs in all three halls versus threshold

4.4 HV scan

In addition to threshold, efficiency also depends on operating HV as well as noise rate, which in turn depends on environment. All RPC modules were tested at 7.6 kV with a threshold of -30 mV for quality assurance before transportation from Beijing to Shenzhen [21]. At Daya Bay, the optimal operating voltage was determined by performing HV scans with a -35mV threshold. During HV scans, the temperature in the experimental halls was controlled to 21.8±1.0 ℃ while the relative humidity of the hall was more than 60%. Of course, the internal humidity of the RPC modules was well below 60% due to the flowing of dry air.

To achieve maximal efficiency for a bare RPC, the operating HV should be at least a few hundred Volts above the knee of the efficiency curve [14]. In contrast, to achieve minimal noise rate and dark current, an operating HV should be as low as possible. Fig. 11 shows the layer efficiency and noise rate curves in each hall. It is seen that the efficiency plateau starts from around 7500 V for EH1 RPCs. By choosing an operating HV of 7600 V, which is several hundred Volts above the knee voltage, we expect that each RPC can reach its optimal efficiency and still allow for fluctuation due to any environmental changes, such as ambient pressure.

The results for EH3 RPCs, shown in the right of Fig. 11, are similar to those for EH1. The decrease in plateau efficiency at higher voltages is an underestimation due to exceedingly higher accidental rates. This feature is not apparent in the two near halls due to their larger signal to background ratios. The lower overall plateau efficiency of EH3 appears in Fig. 11 because the RPC arrays were parked in the RPC halls during commissioning, which prohibits the use of R2 (coincidence with Water Pool) in the efficiency analysis, as discussed in Section 3.2.1.

From the middle of Fig. 11, it is seen that the plateau of EH2 RPCs starts from around 8000V. Comparing with the HV plateau curves of EH1 and EH3, EH2 HV plateau curve moves right. The exact reason will be introduced in Section 4.5. In order to ensure long term stability, EH2 operating HV was also set at 7.6kV.

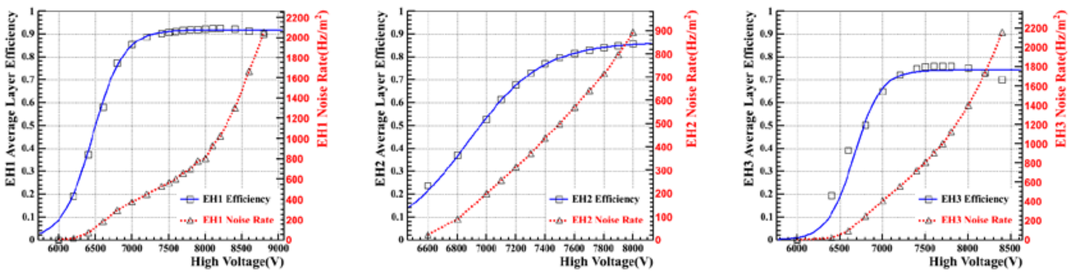

Fig. 11 The average efficiency and noise rate of all layers of RPCs in all three halls versus HV.

4.5 Combined data-taking

Upon completion of all other detectors' commissioning, the RPC arrays were moved over the tops of the water pools, into the designed working position for combined data-taking. In this position, the standard calibration algorithm (including R2) is applied. Fig. 12 a) shows the layer efficiencies of all the layers in each hall, while Fig. 12 b) shows the module efficiencies of all the modules in each hall. Fig. 13 shows the distributions of layer efficiency and module efficiency in each hall. The average layer efficiencies in both EH1 and EH3 are greater than 90%, but the average layer efficiency in EH2 is lower than 90%, which may be caused by an extended period of storage in the highly humid tunnel before installation. The same reason also causes the EH2 HV plateau curve moves right. The mechanism is under investigation. Fig. 14 a) shows the noise rates of all the layers in all three halls, while Fig. 14 b) shows the distributions of layer noise rate in all three halls. The average layer noise rates are 859.6, 954.6 and 727.7 Hz/m^2 in EH1, EH2 and EH3, respectively. In conjunction with the lower efficiency, the higher noise rate (and current) of EH2 RPCs indicate a worse overall performance.

The overall RPC performance in all three halls is summarized in Table 1.

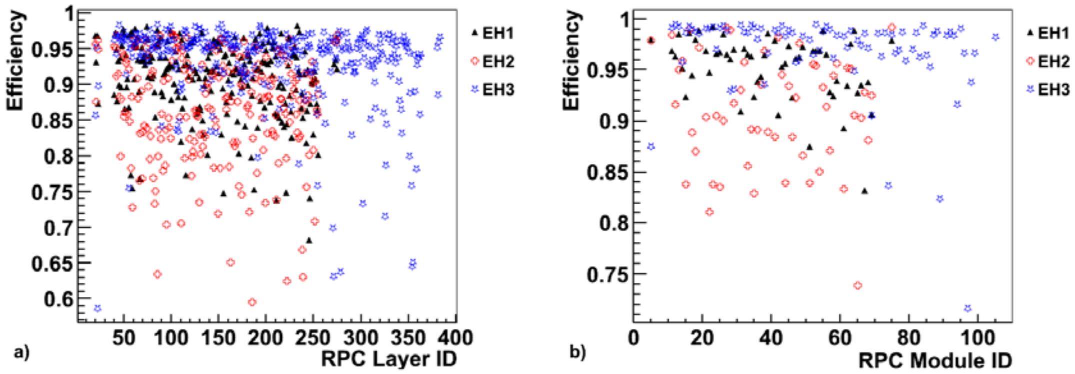

Fig. 12 RPC efficiency versus RPC ID at layer a) and module b) level

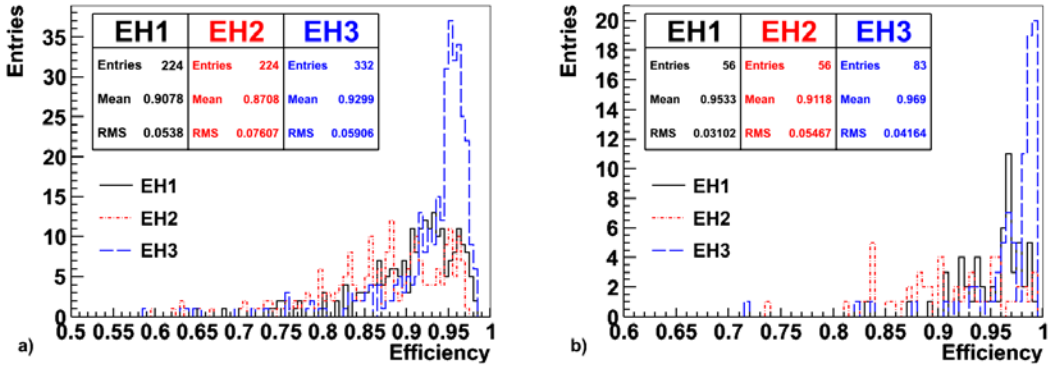

Fig. 13 RPC efficiency distributions at layer a) and module b) level

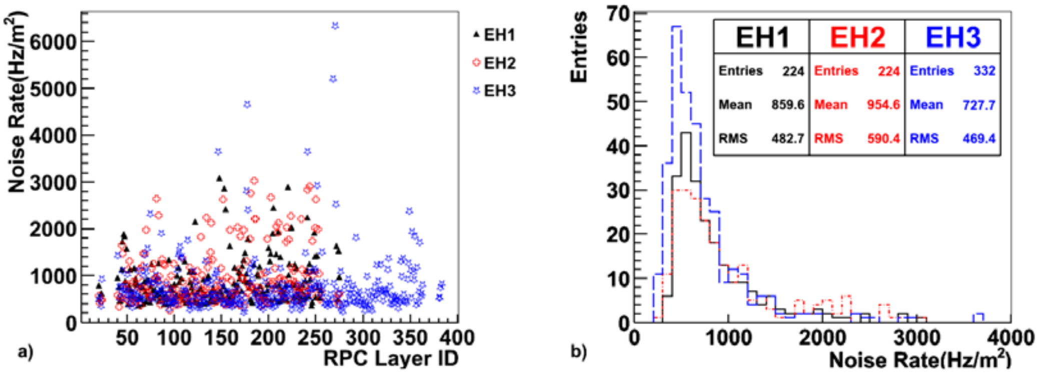

Fig. 14 RPC noise rate: a) Noise rate versus layer ID; b) Noise rate distribution at layer level

Table 1 The RPC average performance in all three halls

Site	Layer Efficiency	Module Efficiency	Noise Rate(Hz/m^2)	Dark Current(μA/ m^2)
EH1	90.78%	95.33%	859.6	4.2
EH2	87.08%	91.18%	954.6	7.6
EH3	92.99%	96.90%	727.7	6.6

5. Summary

Water dropping, high humidity and sparking problems, and so on, were solved to achieve a stable performance for the RPC detectors; especially, the flowing of dry air into RPC modules and the covering of RPC modules, which both ensure long term stability in a severe environment. The specially developed data analysis software provided quick and accurate diagnosis of system performance during commissioning. From HV, threshold and latency scans, operational settings have been optimized. Accordingly, Daya Bay RPC detectors run at 7.6 kV in HV with a signal threshold of -35 mV, a trigger-readout latency of 54 clock cycles and an operating gas flow rate of about 1.0 volumes/day. Combined physics data-taking at all three sites began on December 24, 2011.

6. Acknowledgements

Institute of High Energy Physics, Chinese Academy of Sciences is supported by the China National Science Foundation and the Ministry of Science and Technology of the People's Republic of China. This work is also implemented under Project Y2118M005C supported by the National Natural Science Foundation of China and the Scientific Research Support Plan for New Teachers at Xi'an Jiaotong University. The University of Houston and Princeton University are supported by the United States Department of Energy. Charles University is supported by projects MSM0021620859 and ME08076 of the Ministry of Education, Youth and Sports of the Czech Republic, and 202/08/0760 of the Czech Science Foundation. Finally, we thank Daya Bay shift takers for their help in taking data.

References

[1] Daya Bay Collaboration, Proposal of Daya Bay Experiment, 2007 [arxiv:hep-ex/ 0701029].

[2] Daya Bay Collaboration, Phys. Rev. Lett.108 (2012) 171803.;
Daya Bay Collaboration, http://arxiv.org/abs/1210.6327.

[3] Daya Bay Collaboration, Nucl. Inst. and Meth. A 685 (2012) 78-97.

[4] BaBar,TechnicalDesignReport, SLAC-R-457,March1995.;
F. Anulli, et al, Nucl. Inst. and Meth. A 515 (2003) 322-327.

[5] BELLE Collaboration, A study of CP violation in B meson decays, Technical Design Report, KEK Report 95-1, April 1995.;
BELLE Collaboration, Nucl. Inst. and Meth. A 598 (2009) 183-186.

[6] ALICE Collaboration, TDR of the Muon Spectrometer, CERN/LHCC 99-22, 1999.;
ALICE collaboration, Nucl. Inst. and Meth. A 661 (2012) 45-49.

[7] ATLAS Muon Collaboration, ATLAS Muon Technical Design Report, CERN/ LHCC 97-22, 1997.;
ATLAS Muon Collaboration, Nucl. Inst. and Meth. A 661 (2012) 6-9.

[8] CMS Collaboration, Muon Project, CERN/LHCC 97-32, 1997.;
G. Roselli, et al, Nucl. Inst. and Meth. A 602 (2009) 696-699.

[9] R. Santonico, et al., Nucl. Instr. and Meth. A 187 (1981) 377-380.

[10] J. Zhang, et al., Nucl. Instr. and Meth. A 540 (2005) 102-112.

[11] Y. Xie, et al., Nucl. Instr. and Meth. A 599 (2009) 20-27.

[12] J. Zhang, et al., Nucl. Instr. and Meth. A 614 (2010) 196-205.

[13] Q. Zhang et al., Nucl. Instr. and Meth. A 583 (2007) 278–284.

[14] L. Ma, et al., Nucl. Instr. and Meth. A 659 (2011) 154–160.

[15] L. Ma, et al., Chin. Phys. C (HEP & NP) 34 (8) (2010) 1116-1121.

[16] http://www.caentechnologies.com/csite

[17] H. Hao et al., Development of VME system in RPC electronics for Daya Bay Reactor Neutrino Experiment, Nuclear Science and Techniques (Accepted, in press)

[18] F. Li, et al., IEEE Transactions on Nuclear Science NS-58 (4) (2011) (2011) 1723-1727.

[19] Q. Zhang et al., Offline Software of RPC Detector System in Daya Bay Reactor Neutrino Experiment, accepted by Journal of Physics: conference series

[20] http://escholarship.org/uc/item/6jm8g76d

[21] http://cern.ch/gaudi/

[22] http://dayabay.bnl.gov/dox/LafKernel/html/annotated.html

[23] J. Xu, et al., Chin. Phys. C (HEP & NP) 35 (9) (2011) 844-850.